Some Complexities in the Reaction of Hydrogen Atoms Generated in H_2 Discharge with Molecular Chlorine

Otto Dobis and Sidney W. Benson*

Loker Hydrocarbon Research Institute, University of Southern California, University Park, Los Angeles, California 90089-1661

Received: November 30, 2001; In Final Form: February 18, 2002

The kinetics of the reaction $H + Cl_2 \xrightarrow{1} HCl + Cl$ has been studied in the very low-pressure reactor (VLPR) system at 298 K using two different H atom generation sources. The first one is the microwave decomposition of HCl giving $k_1 = (8.66 \pm 0.18) \times 10^{-12}$ cm^3/(molecule-s). No traces of HCl(v) excited product side reaction could be found in the system due to the much longer residence time in the reactor than the spontaneous decay of excited HCl. The second H atom source is the microwave decomposition of H_2. This technique produces 5% $H_2(v)$ which initiates the reaction $Cl + H_2(v) \xrightarrow{2} HCl + H$, hydrogen atom recovery and the quenching reaction, $H + H_2(v) \xrightarrow{tr} H_2 + H$. They are identified by differences in the HCl and Cl yields, as well as from the extra H_2 consumption. Rate constants $k_2 = (2.88 \pm 0.13) \times 10^{-11}$ and $k_{tr} = (2.95 \pm 0.17) \times 12^{-12}$ cm^3/(molecule-s) are measured along with excellent mass balances between reactant consumption and product formation. Consideration of the high value found for k_{tr} leads to the conclusion that its mechanism is by atom transfer rather than collisional deactivation. Both rate constants agree well with the corresponding *A*-factors reported for thermal reactions indicating that the vibrational excitation energy of $H_2(v)$ provides the activation energies of the thermal reactions.

Introduction

The fast, exothermic reaction

$$H + Cl_2 \xrightarrow{a} HCl(v) + Cl \quad -45.2 \text{ kcal/mol}$$

represents a very complex kinetic system to establish a reliable thermal rate constant for this apparently simple chemical step. Due to its broad theoretical and practical interest, a large number of experimental studies have been devoted to this kinetic problem without reaching consensus. In a previous report,[1] we have compiled the related experimental results (Table 1 in ref 1) which shows that the reported rate constants vary by a factor 9 by ranging from 0.39×10^{-11} up to 3.5×10^{-11} cm^3/(molecule-s). Our analysis of those data pointed out two sources of experimental difficulties in the kinetic investigation of this reaction:

1. The formation of the highly reactive HCl(v) product. The first vibrational excitation state ($v = 1$) has 8.2 kcal/mol extra energy which well exceeds the 3.4 kcal/mol activation energy[2] requirement for the H + HCl reaction, thereby initiating a rapid H atom consumption in competition with HCl(v) quenching on the short contact time scale (1−15 ms) used in fast flow experimental systems.

2. All flow systems used for absolute rate constant measurements use the partial microwave decomposition of H_2 for H atom generation. This technique also produces excited $H_2(v)$ in an unknown ratio[3] of the initial H_2 flow. It will then react with the Cl atom product of reaction (a) invoking the chain recovery of H atom in a presumably fast process.

These complexities involving vibrationally excited species make it impossible to set a reliable stoichiometry for the H atom consumption kinetics. But they can be suppressed or isolated in specially designed experimental runs in the very low-pressure reactor (VLPR) system.

It was shown earlier[4] that the HCl residence time in the reactor cell of the VLPR system is at least 20 times longer than the spontaneous radiation decay time of HCl($v = 1$). H atoms and especially Cl atoms may also contribute to HCl(v) quenching. Therefore, we could never observe any traces of HCl(v) reaction[4] in our system. Now using the microwave partial decomposition of HCl for H atom generation and reacting it with Cl_2, the investigation of the pure thermal reaction

$$H + Cl_2 \xrightarrow{1} HCl + Cl$$

is established for the measurement of k_1. Knowing the thermal rate constant k_1, we can substitute the HCl/H atom source by the microwave partial decomposition of H_2 and explore the kinetic perturbations arising from the presence of $H_2(v)$ in the same system. These are the objectives of our present experimental studies.

Experimental Section

The VLPR system used for the present measurements is the same three-stage, all-turbo-pumped equipment we have used for previous studies.[1] It has been described in detail earlier.[5] For a short survey of its present application, a brief summary of the system parameters, experimental sequence, and data processing is given in the following.

A new, thin Teflon-coated, cylindrical, thermostated flow cell reactor of volume $V_r = 216.5$ cm^3 is sealed at its bottom to the

* Corresponding author.

10.1021/jp014385z CCC: $22.00
Published on Web 04/04/2002

TABLE 1: HCl Decomposition and Recombination of Cl Atoms Using Φ_2 Orifice and an Initial Flow of $[HCl]_i k_{eHCl} = 5.43 \times 10^{12}$ molecules/(cm^3-s)

microwave power, W	$I_{35}/(I_{35}+I_{36}) \times 10^2$, %	$[Cl_2]k_{eCl} \times 10^{-10}$	$2[Cl_2]k_{eCl_2}/[HCl]_i k_{eHCl} \times 10^2$, %
20	56.16 ± 0.34	1.86	0.68
30	56.46 ± 0.58	1.43	0.53
40	58.69 ± 0.29	1.05	0.38
50	60.12 ± 0.42	0.94	0.35
55	59.52 ± 0.38	1.14	0.42
60	60.15 ± 0.45	1.00	0.37
65	59.12 ± 0.10	0.99	0.36
70	59.85 ± 0.21	1.04	0.38

TABLE 2: Initial and Final Steady-State Concentrations[a] of Cl_2 Reactant and of Cl and HCl Products in Reaction 1[b]

no./Φ_x	$[Cl_2]_0$	$[Cl_2]$	[Cl]	[HCl]	initial conditions
1/Φ_2	2.18	0.27	5.21	4.07	nos. 1−7/Φ_2:
2/Φ_2	3.01	0.43	5.66	4.53	$[HCl]_i = 6.61$
3/Φ_2	3.76	0.58	6.06	5.05	$10^2 I_{35}/(I_{35}+I_{36}) = 59.12 \pm 0.10\%$
4/Φ_2	4.58	0.93	6.43	5.32	$[Cl]_0 = 3.86$
5/Φ_2	5.64	1.32	6.92	5.73	$[HCl]_0 = 2.70$
6/Φ_2	9.82	4.42	7.64	6.46	$[H]_{Cl} = 0.65$[c]
7/Φ_2	12.88	7.27	7.81	6.77	
8/Φ_3	0.70	0.18	2.51	1.63	nos. 8−15/Φ_3:
9/Φ_3	1.13	0.32	2.72	1.88	$[HCl]_i = 3.44$
10/Φ_3	1.57	0.47	2.96	2.09	$10^2 I_{35}/(I_{35}+I_{36}) = 63.27 \pm 0.27\%$
11/Φ_3	2.06	0.71	3.08	2.22	$[Cl]_0 = 2.14$
12/Φ_3	2.93	1.06	3.42	2.59	$[HCl]_0 = 1.26$
13/Φ_3	5.72	2.98	4.03	3.20	$[H]_{Cl} = 0.36$[c]
14/Φ_3	8.45	5.04	4.23	3.41	
15/Φ_3	11.58	8.45	4.40	3.55	
16/Φ_5	0.21	0.12	1.04	0.50	nos. 16−22/Φ_5:
17/Φ_5	0.37	0.22	1.08	0.54	$[HCl]_i = 1.42$
18/Φ_5	0.57	0.35	1.14	0.60	$10^2 I_{35}/(I_{35}+I_{36}) = 69.56 \pm 0.23\%$
19/Φ_5	0.85	0.53	1.24	0.66	$[Cl]_0 = 0.97$
20/Φ_5	1.21	0.77	1.30	0.76	$[HCl]_0 = 0.43$
21/Φ_5	2.35	1.62	1.54	0.98	$[H]_{Cl} = 0.16$[c]
22/Φ_5	4.10	3.05	1.74	1.19	

[a] All concentrations are in units of 10^{12} particles/cm^3. [b] H atom source is the microwave decomposition of HCl. [c] $[H]_{Cl}$ is the initial concentration of H atoms generated by HCl decomposition calculated as $[H]_{Cl} = [Cl]_0 k_{eCl}/k_{eH}$.

top of the main vacuum chamber. Gas inlets are affixed on the top of the reactor preceded by resistive capillary flow subsystems calibrated for regulating the inlet fluxes of initial gas components with the use of Validyne transducers. Two gas inlets are used in the present series of measurements. One of the inlets is connected through a detachable phosphoric acid coated quartz discharge tube centered in the Opthos microwave generator cavity of a McCarrol antenna before joining at the tapered capillary inlet of the reactor cell. This feed-through is used for a 3.8% HCl/He gas mixture inlet flow in the first series of experiments and then for a 4.7% H_2/He gas composition controlled flow in the second series of runs. The other separate supply line serves for a 10% Cl_2/He gas mixture inlet flow that provides the variable Cl_2 reactant concentration for reaction 1 in the reactor cell.

The reactor base is seated on a Teflon-coated, rapidly adjustable slide[5] having three interchangeable escape orifices with diameters of 0.193, 0.277, and 0.485 cm. Their use in different runs is indicated as Φ_2, Φ_3, and Φ_5, respectively, in Table 2 and marked with different symbols in Figures. With the above reactor volume V_r, the first-order escape rate constant for any gas component of mass M is given by $k_{eM} = a_\phi (T/M)^{1/2}$ s^{-1}, where T is the absolute temperature and $a_\phi = 0.285$ for Φ_2, 0.549 for Φ_3, and 1.334 for Φ_5 orifices. All escape rate constants appearing in kinetic equations later on were calculated according to the above formula. The stepwise switch-over of orifices changes the values of the first-order escape rate constants of gases which allows the variation of the reactor residence time by a factor of 4.7.

The well-controlled gas inlet and outlet dynamics establishes the strictly defined steady-state flow condition in the reactor that operates in the Knudsen flow regime. The uncertainty in flow is less than 1% and is incorporated in the overall scatter of measured data.

The gas mixture of products and unreacted reagents leaves the reactor cell in the form of an effusive molecular beam through one of the selected exit orifices. This beam is chopped by a tuning fork and further collimated by two successive pinholes in the differentially pumped vacuum system to reduce the background mass signal. The beam is sampled with the off-axis mass analyzer of the quadrupole mass spectrometer and the mass signals are fed to a phase sensitive lock-in amplifier tuned to the chopping frequency. This chopping modulated phase sensitive detection ensures that we are sampling species which have not made collisions after leaving the reactor. The measured mass ranges are repeatedly scanned, usually 20−30 times, to give a good statistical average and the mass intensities are recorded for data acquisition. Each mass signal is corrected for any small background value recorded prior to start-up of mass flow.

Mass spectral calibration for a given molecular gas component of mass M is carried out by measuring the mass signal intensity I_M as a function of the specific flux $F(M)$ according to the relationship $I_M = \alpha_M F(M)$, where α_M is the mass spectral efficiency for mass M and $F(M) =$ flux/V_r in units of molecules/(cm^3-s). This relationship is strictly linear in the mass flow range of our experiments. The steady-state concentration of the gas component M in the reactor cell can then be calculated from the relation $[M] = F(M)/k_{eM}$.

Mass spectral calibration for HCl was carried out in the flow range of $(0.49-9.58) \times 10^{12}$ molecules/(cm^3-s) giving $\alpha_M = (3.783 \pm 0.075) \times 10^{-11}$ with a negligibly small Cl/HCl fragmentation ratio of 0.30 ± 0.11% using 20 eV electron energy. It is almost four times more sensitive with 40 eV spectrometry giving $\alpha_M = (1.424 \pm 0.026) \times 10^{-10}$, but the fragmentation ratio is 7.59 ± 0.36% for which the measured I_{Cl} signal intensities are corrected before converting them into [Cl] concentrations. The Cl atom flow measurement is based on the total balance of Cl and HCl signal intensities studied in detail earlier using absolute mass signal intensity measurements[6] which sets $\alpha_{Cl} = \alpha_{HCl}$ within a ±2% scatter.

The Cl_2 mass spectrometry in our system is reported earlier.[1] Its Cl atom fragmentation ratio of 0.67% with 20 eV and 3.56% with 40 eV electron energy involves a second correction to the Cl mass signal produced in reaction 1.

Mass spectral sensitivity for low masses, like those of H and H_2 is very poor. Even with 40 eV spectrometry the H atom signal at mass 1 appears as inconclusive small traces, almost indistinguishable from the background signal. Therefore, the initial $[H]_0$ concentration is derived from the HCl decomposition as will be shown. H_2 is measurable at mass 2 with low efficiency and with relatively high scatter. Its flow calibration gives $a_{H_2} = (6.60 \pm 0.29) \times 10^{-13}$ with 40 eV ionization energy.

Results

The microwave decomposition of HCl is a new method of free atom generation in our VLPR system. Therefore, this decomposition was studied first using Φ_2 exit orifice and a

stepwise increase of the microwave power. The reason for using Φ_2 orifice is that wall recombination products, if any, would likely appear at the longest residence time.

HCl initial flow of 5.431×10^{12} molecules/(cm^3-s) was started up and mass range of 35−38 repeatedly scanned recording the signal intensities of Cl and HCl as well as their isotopes with 20 and 40 eV spectrometry. It is a regular procedure with the start of every run to check the constancy of mass spectral sensitivity using the known HCl flow as standard. Then the microwave generator is turned on and its power regulated in steps between 20 and 70 W. Mass ranges of 35−38 and 70−74, the only new small signals of Cl_2 in the spectrum, are scanned with each power setting. The results, summarized in Table 1, show that an almost uniform HCl decomposition of $59.6 \pm 0.3\%$ can be achieved in the microwave power range 40−70 W. In this range, only a very small part of the initial HCl, $0.38 \pm 0.02\%$, is converted into Cl_2 product. Since the Cl_2 product ratio is somewhat higher at low microwave power, it indicates that the Cl atom recombination occurs in the discharge tube rather than in the reactor cell. Also, the Cl atom recombination increases slightly with the aging of the discharge tube. It reaches about 1% after running the microwave discharge for 50 h. Therefore, the discharge tube is regularly recoated with H_3PO_4 after 40 h service.

It is assumed that the HCl decomposition provides an equal amount of H atom per Cl atom formed or HCl decomposed. This can be tested experimentally by measuring the flow balance of Cl_2 consumption against HCl and Cl product formations in reaction 1.

After recording the initial conditions set by the initial flow and the microwave decomposition of HCl (see the last column of Table 2), gradually increased flow of the 10% Cl_2/He gas composition is introduced through the second inlet which corresponds to the $[Cl_2]_0$ initial concentrations given in the second column of Table 2. Then the actual concentrations of Cl_2, Cl, and HCl were measured in each step using both 20 and 40 eV mass spectrometry. Their values averaged for both electron energy measurements are given in Table 2.

Reaction 1 provides four steady-state flow equations, two for the reactants consumed and two for the products formed:

$$([H]_0 - [H])k_{eH} = -\Delta[Cl]k_{eCl} = -\Delta[HCl]k_{eHCl} = \Delta[Cl_2]k_{eCl_2} = k_1[H][Cl_2] \quad (1)$$

Note that both Cl and HCl products increase with the progress of reaction 1, so their changes are negative according to the convention $\Delta[Cl] = [Cl]_0 - [Cl]$ and $\Delta[HCl] = [HCl]_0 - [HCl]$. The mass balance between Cl and HCl products is presented in Figure 1. The good equality found suggests that the average of product formation as $(\Delta[Cl]k_{eCl} + \Delta[HCl]k_{eHCl})/2$ can be used further on. It takes account for the overall scatter of product formation. The balance between Cl_2 reactant consumption and product formation is shown in Figure 2. These Figures represent an excellent mass balance based exclusively on reaction 1.

Expressing the H atom concentration from the last equality in eq 1 as $[H] = \Delta[Cl_2]k_{eCl_2}/k_1[Cl_2]$ and substituting it into the first equality of H atom consumption, a steady-state kinetic equation for the relative Cl_2 consumption in the function of product formation is obtained as

$$\frac{\Delta[Cl_2]}{[Cl_2]}k_{eCl_2} = k_1[H]_0 + \frac{k_1}{k_{eH}}\left(\frac{\Delta[Cl]k_{eCl} + \Delta[HCl]k_{eHCl}}{2}\right) \quad (2)$$

where the slope is proportional to k_1 and the intercept to the

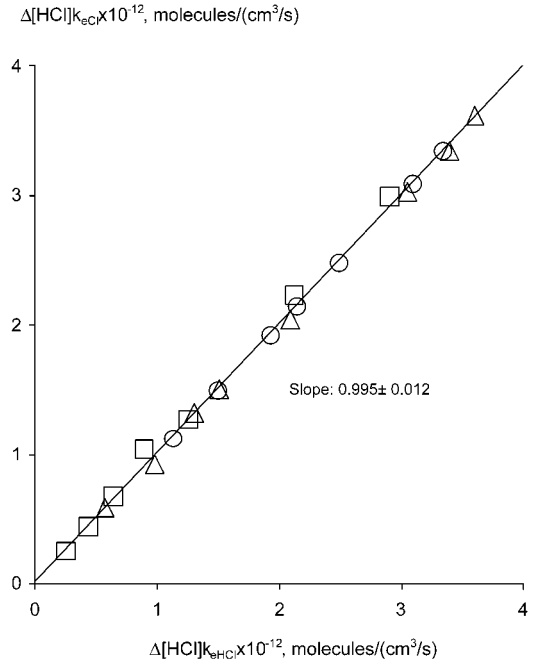

Figure 1. Mass flow balance between Cl atom and HCl product formations plotted according to eq 1. Symbols of orifices for data pairs are: O, Φ_2; Δ, Φ_3; □, Φ_5.

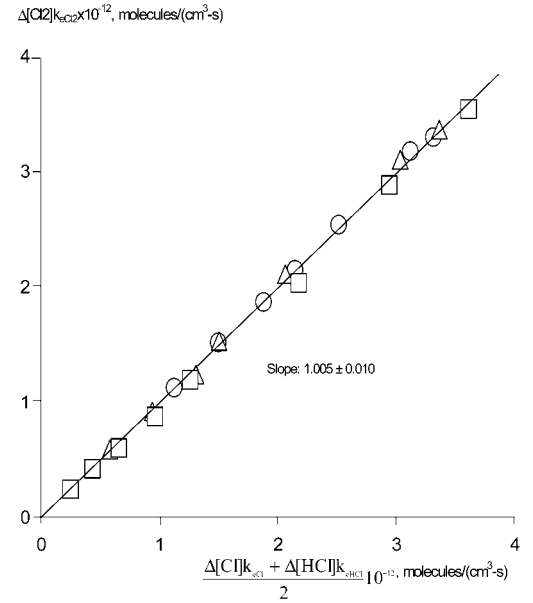

Figure 2. Mass flow balance between Cl_2 consumption and Cl + HCl product formations in reaction 1 plotted according to eq 1. Symbols of orifices are the same as in Figure 1.

initial H atom concentration. Note that both the Cl atom and HCl concentrations are increasing with the progress of reaction 1. Therefore, their changes are negative by the convention $[X]_0 - [X] = \Delta[X]$, where X is either Cl or HCl. The plot of measured data according to eq 2 is presented in Figure 3.While the evaluation of k_1 shows good agreement within the scatters for all three orifices, the obtained $[H]_0$ concentrations are somewhat higher than calculated from the initial $[Cl]_0$ concentrations given in the last column of Table 2. The $[H]_0 - [H]_{Cl}$ differences are: 7.22×10^{10} for Φ_2, 7.37×10^{10} for Φ_3, and 7.03×10^{10} atoms/cm^3 for Φ_5 orifices. It indicates that our experimental system has a small, permanent, background H atom concentration calculated as $[H]_b = [H]_0 - [H]_{Cl} = (7.2 \pm 0.2) \times 10^{10}$ atoms/cm^3 which is independent of the exit orifice size

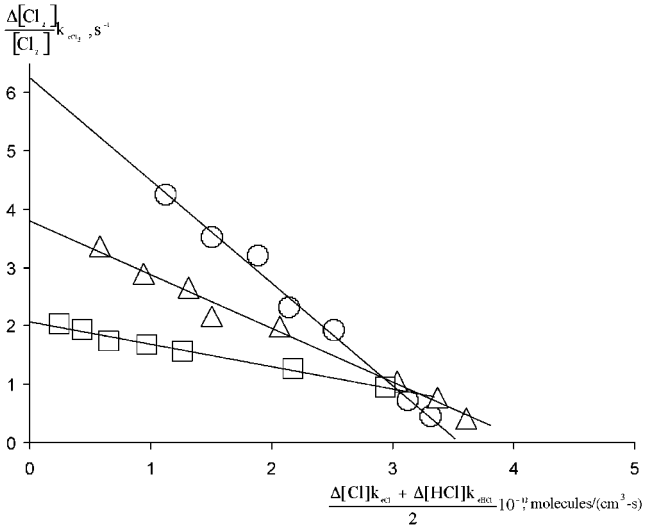

Figure 3. Relative Cl_2 consumption vs the average of Cl and HCl product formation plotted according to eq 2. Symbols of orifices are the same as in Figure 1. The slopes and intercepts are proportional to k_1 cm^3/(molecule-s) and $[H]_0$ atoms/cm^3, respectively. Evaluation give $k_1 = (8.64 \pm 0.38) \times 10^{-12}$ and $[H]_0 = (7.24 \pm 0.33) \times 10^{11}$ for Φ_2, $k_1 = (8.71 \pm 0.89) \times 10^{-12}$ and $[H]_0 = (4.36 \pm 0.19) \times 10^{11}$ for Φ_3, and $k_1 = (8.81 \pm 0.54) \times 10^{-12}$ and $[H]_0 = (2.34 \pm 0.15) \times 10^{11}$ for Φ_5 measurements.

and is present only when the microwave discharge is on. This background H atom concentration originates from the decomposition of the H_3PO_4 coat of the discharge tube.[1] Depending on the orifice size used, it constitutes 10−30% of the initial H atom concentration.

With the knowledge of the above corrected initial H atom concentrations, the rate constant k_1 can now be recovered from the relationship of the relative Cl_2 consumption with the actual H atom concentration:

$$\frac{\Delta[Cl_2]}{[Cl_2]}k_{eCl_2} = k_1\left([H]_0 + \frac{\Delta[Cl]k_{eCl} + \Delta[HCl]k_{eHCl}}{2k_{eH}}\right) \quad (2a)$$

The plot of experimental data according to eq 2a is presented in Figure 4. Measurements made with all three exit orifices lead to a good uniform straight line whose slope gives

$$k_1 = (8.66 \pm 0.18) \times 10^{-12}\ \text{cm}^3/(\text{molecule-s})$$

In the second series of experiments, the H atom generation is replaced for the microwave decomposition of H_2 using a 4.7% H_2/He gas composition flowing through the discharge tube. These experimental runs are carried out with a permanent initial flow of H_2 which corresponds to $[H_2]_I = 2.111 \times 10^{12}$ molecules/cm^3 in the reactor cell using Φ_3 orifice. The microwave decomposition of H_2 is less effective than that of HCl. It is 42.0−53.4% in the microwave power range of 50−70 W. The measured concentrations of reactants and products are summarized in Table 3, where Cl_2, Cl, and HCl concentrations are the averages of 20 and 40 eV mass spectrometry, while H_2 concentrations are measured with 40 eV only.

Analysis of mass flow balances indicates that the Cl_2 consumption is in good accordance with Cl and HCl product formation presented in Figure 5. Nevertheless, the HCl and Cl products shown in Figure 6, exhibit some deviation from equalty. Due to hitherto unknown side reactions, some extra

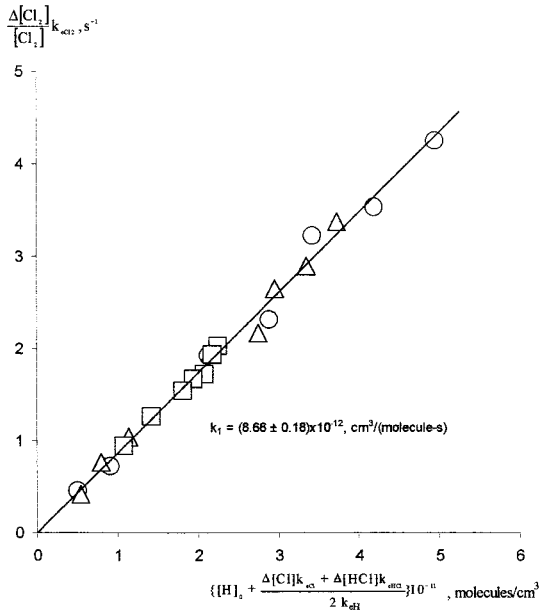

Figure 4. Relative Cl_2 consumption vs the H atom concentration plotted according to eq 2a. The slope gives k_1 directly. Symbols of orifices are the same as in Figure 1.

TABLE 3: Initial and Final Steady-State Concentrations[a] of Reactants and Products in Reactions 1−3; H Atom Source Is the Microwave Decomposition of H_2[b]

no.	$[Cl_2]_0$	$[Cl_2]$	[HCl]	[Cl]	$[H_2]_0$	$(I^i_{H_2} - I^0_{H_2})/I^i_{H_2}$	$[H_2]$	$(I^i_{H_2} - I_{H_2})/I^i_{H_2}$
1	0.98	0.31	0.85	0.50	1.23	0.420	1.18	0.440
2	1.13	0.35	0.94	0.63	1.10	0.477	1.08	0.490
3	1.57	0.53	1.20	0.87	1.05	0.505	1.02	0.517
4	2.06	0.75	1.49	1.13	1.05	0.505	0.99	0.529
5	2.61	1.03	2.00	1.69	0.98	0.534	0.93	0.561
6	2.93	1.14	2.05	1.69	1.10	0.477	1.07	0.495
7	5.72	2.81	3.92	3.54	1.05	0.505	1.02	0.519
8	8.82	5.72	5.99	5.51	0.98	0.534	0.95	0.549
9	11.58	10.61	7.92	7.28	1.23	0.420	1.16	0.449
10	15.09	19.88	10.23	9.50	1.10	0.477	1.02	0.515
11	17.95	32.82	11.62	10.77	0.98	0.534	0.92	0.566

[a] $[Cl_2]$ final state concentration is in unit of 10^{11} molecules/cm^3. All other concentrations are in units of 10^{12} particles/cm^3. [b] Initial H_2 flow (without running the microwave discharge) corresponds to $[H_2]_i = 2.11 \times 10^{12}$ molecules/cm^3, its mass signal intensity is $I^i_{H_2}$.

HCl is formed and/or a small part of Cl product is converted to HCl.

Neglecting the above deviation and employing eq 2 for the kinetic presentation of data given in Table 3, a curved relationship shown with broken line in Figure 7 is obtained. It clearly indicates that the kinetics cannot be described by a single-step reaction mechanism attributed to eq 2. At the same time, Figure 7 illustrates some sources of variances in k_1 values found in the literature. The slope determined by the first six points, where conditions $[H]_0 \geq [Cl_2]_0$ prevails, gives $k_1 = (2.9 \pm 0.5) \times 10^{-11}$ cm^3/(molecule-s). This value is in agreement[3] with $k_1 = (3.5 \pm 1.2) \times 10^{-11}$ and $(3.0 \pm 1.6) \times 10^{-11}$ cm^3/(molecule-s)[7] measured under the conditions of high H/Cl_2 ratios. On the other hand, the slope determined by the last three data points, where the initial conditions are $[Cl_2]_0 > [H]_0$, gives $k_1 = (1.0 \pm 0.1) \times 10^{-11}$ cm^3/(molecule-s) approaching the low k_1 value derived from the former experimental technique.

The results shown in Figures 6 and 7 require a multistep reaction mechanism which takes account of the Cl < HCl product formation and the extra H_2 consumption with the

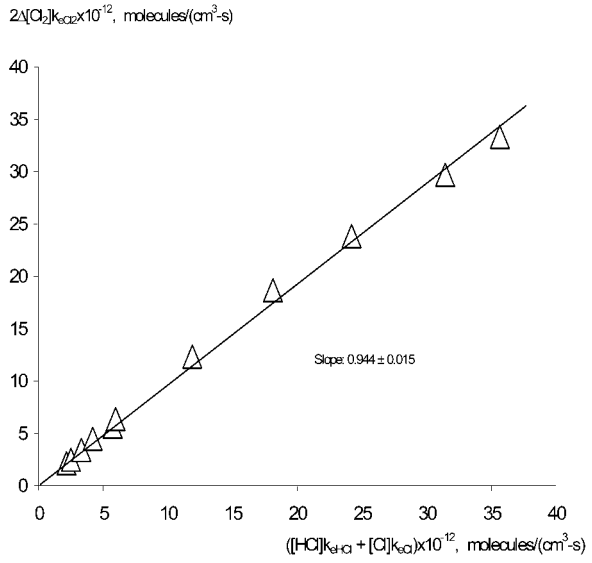

Figure 5. Mass flow balance between Cl_2 consumption and Cl + HCl product formation using H_2 decomposition for H atom source.

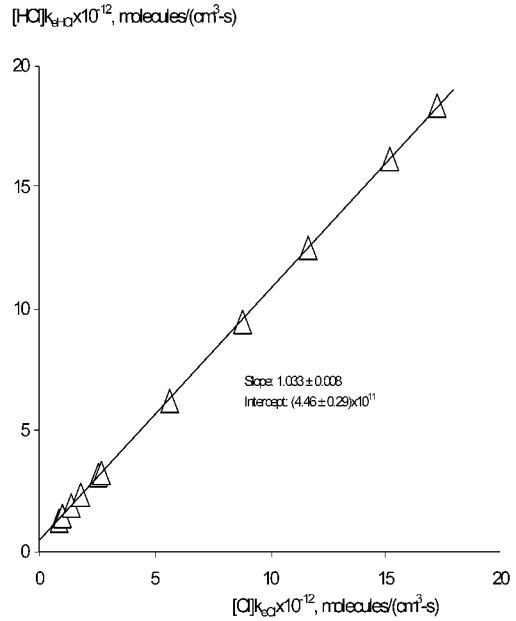

Figure 6. Mass flow balance between HCl and Cl product formations using H_2 decomposition for H atom source.

progress of reaction 1 shown in columns 8 and 9 of Table 3. In principle, both deviations could be described by the Cl atom reaction with undecomposed H_2, but, with ground state thermal H_2, this reaction is slow and makes only a small part of corrections to the kinetics. Vibrationally excited H^*_2 formed in the microwave discharge has a long life span[12] and enhanced reactivity with Cl. The following reactions are thus added to eq 1:

$$H^*_2 + Cl \xrightarrow{2} HCl + H$$

$$H_2 + Cl \xleftrightarrow{3} HCl + H$$

$$H^*_2 + H \xrightarrow{tr} H_2 + H$$

The rate of reaction 2 is unknown. Equilibrium 3 is a well-established process. The rate constant for the forward reaction[8]

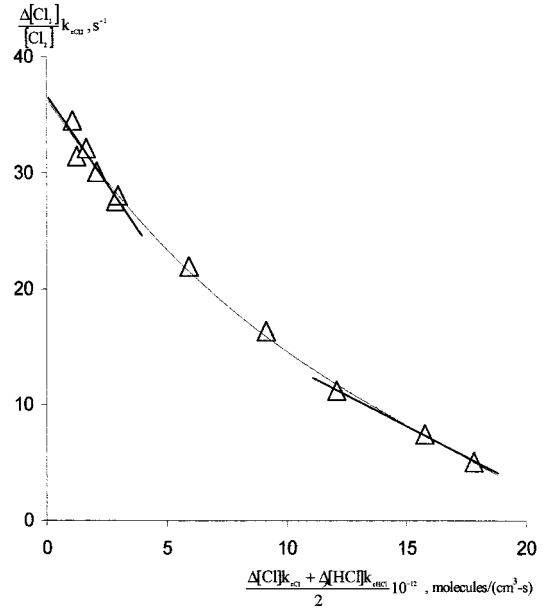

Figure 7. Relative Cl_2 consumption vs the average of Cl and HCl formation plotted according to eq 2.

is $k_3 = 1.6 \times 10^{-14}$ cm^3/(molecule-s), while that for the backward reaction[9] is $k_{-3} = 4.1 \times 10^{-14}$ cm^3/(molecule-s). The equilibrium constant: $K_{-3} = 2.5$ is very well-known. Excited H^*_2 products with high vibrational levels, $v > 1$, are produced in a very small ratio[10] in the microwave discharge and rapidly relaxed to $v = 1$. $H_2(v=1)$ is a long-lived excited state. Its quenching is slow with molecular colliders. Even with HCl, it has a rate coefficient[11] of 4×10^{-14} cm^3/(molecule-s) and about 3 orders of magnitude less[12] with H_2. But H atom is found to be an effective collision partner[13] through H atom exchange reaction with a rate constant of $(5.2 \pm 0.2) \times 10^{-12}$ cm^3/(molecule-s).

The above extended mechanism provides the following steady-state equations for reactant consumption and product formations. For HCl formation:

$$[HCl]k_{eHCl} = (k_1[Cl_2] - k_{-3}[HCl])[H] + (k_2[H^*_2] + k_3[H_2])[Cl] \quad (3)$$

For Cl consumption:

$$[Cl]k_{eCl} = (k_1[Cl_2] + k_{-3}[HCl])[H] - (k_2[H^*_2] + k_3[H_2])[Cl] \quad (4)$$

For Cl_2 consumption:

$$\Delta[Cl_2]k_{eCl_2} = k_1[H][Cl_2] \quad (5)$$

For H^*_2 consumption:

$$\Delta[H^*_2]k_{eH_2} = (k_2[Cl] + k_{tr}[H])[H^*_2] \quad (6)$$

For H_2 consumption:

$$\Delta[H_2]k_{eH_2} = (k_2[H^*_2] + k_3[H_2])[Cl] - k_3K_{-3}[H][HCl] \quad (7)$$

where $\Delta[H_2] = [H_2]_0 - [H_2]$, the difference of data of columns 6 and 8 in Table 3.

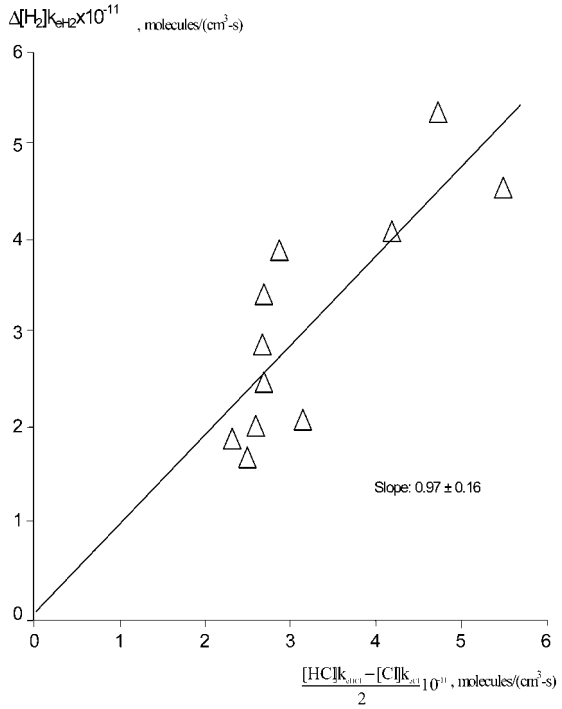

Figure 8. H_2 consumption in reactions 2 and 3 plotted according to eq 10.

The steady-state concentrations, which are not measurable directly, like H^*_2, can be derived from eqs 3 and 4:

$$[H_2^*] = \frac{[HCl]k_{eHCl} - [Cl]k_{eCl}}{2k_2[Cl]} + \left(K_{-3}[H]\frac{[HCl]}{[Cl]} - [H_2]\right) \quad (8)$$

and H from the rearrangement of eq 5:

$$[H] = \frac{\Delta[Cl_2]k_{eCl_2}}{k_1[Cl_2]} \quad (9)$$

Substituting eqs 8 and 9 into eq 7 a flow balance equation

$$\Delta[H_2]k_{eH_2} = \frac{[HCl]k_{eHCl} - [Cl]k_{eCl}}{2} \quad (10)$$

is obtained. The corresponding data of Table 3 are plotted according to this equation in Figure 8.

Due to small changes (the order of 10^{11}) in flow rate differences and the low efficiency of H_2 mass spectrometry, the relatively large scatter (±16%) is anticipated. The slope is consistent with the H_2 consumption and the extra HCl formation. Note that the origin is a valid point on this line.

Multiplying eq 6 by two and substituting H^*_2 and H concentrations from eqs 8 and 9, a general steady-state kinetic equation can be derived in the form:

$$[HCl]k_{eHCl} - [Cl]k_{eCl} + 2k_3\left(K_{-3}\frac{\Delta[Cl_2]k_{eCl_2}}{k_1[Cl_2]}[HCl] - [H_2][Cl]\right) = 2[H_2^*]_0k_{eH_2} - \frac{1}{k_2}\left(\frac{k_{tr}}{k_1} \times \frac{\Delta[Cl_2]k_{eCl_2}}{[Cl_2]} + k_{eH_2}\right)\left\{\frac{[HCl]k_{eHCl} - [Cl]k_{eCl}}{[Cl]} + 2k_3\left(K_{-3}\frac{\Delta[Cl_2]k_{eCl_2}}{k_1[Cl_2]} \times \frac{[HCl]}{[Cl]} - [H_2]\right)\right\} \quad (11)$$

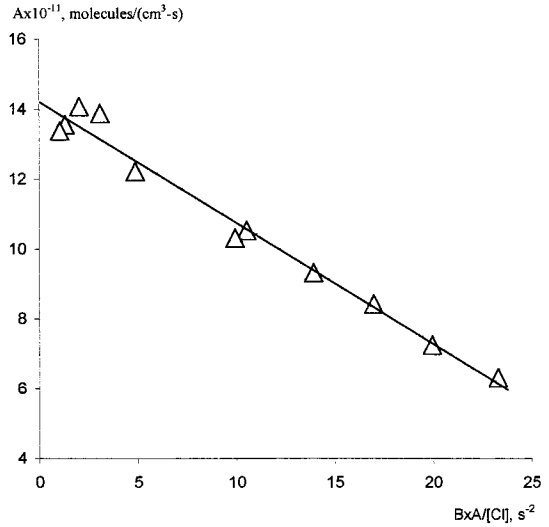

Figure 9. Kinetics of $H_2(v = 1)$ + Cl reaction derived from the total mechanism of reactions 1−3 and the energy transfer process. Data are plotted according to eq 11a using the optimalized ratio of $k_1/k_{tr} = 0.34$. The slope is directly proportional to $-1/k_2$ and the intercept is $2[H_2](v = 1)]_0k_{eH_2}$.

For practical computational treatment, this complex equation can be written in the short form:

$$A = 2[H_2^*]_0k_{eH_2} - \frac{1}{k_2}B \times A/[Cl] \quad (11a)$$

where A and B are the obvious sets of constants and variables given in eq 11. Its linear form would permit the calculation of k_2 as the inverse of the slope and of the initial $[H^*_2]_0$ concentration from the intercept.

For numerical calculations of A and B, the data of Table 3, k_1 measured in the first series of experiment (shown in Figure 4), as well as k_3 and K_{-3} values[8,9] are used. Since the ratio of k_{tr}/k_1 is a significant factor of linearity and the referred[13] k_{tr} value does not fit precisely to that requirement, eq 11 was subjected to linear regression by varying k_{tr}/k_1 between 0.2 and 0.6. The best fit is obtained with

$$k_{tr}/k_1 = 0.34 \pm 0.02$$

which yields the rate constant of the vibrational energy transfer process to

$$k_{tr} = (2.95 \pm 0.17) \times 10^{-12}\ cm^3/(molecule\text{-}s)$$

Using the above ratio for the calculation of B and plotting the data according to eq 11, the linear relationship presented in Figure 9 is obtained. The intercept corresponds to

$$[H^*_2]_0 = (1.06 \pm 0.02) \times 10^{11}\ molecules/cm^3$$

which is 5% of the $[H_2]_i$ initial concentration. The slope gives

$$k_2 = (2.88 \pm 0.13) \times 10^{-11}\ cm^3/(molecule\text{-}s)$$

which indicates that reaction 2 is 1800 times faster than reaction 3 at room temperature.

Discussion

The microwave decomposition of HCl proved to be the most appropriate H atom source to investigate the kinetics of reaction

1 in our VLPR system. The equal distribution of Cl and HCl products shown in Figure 1 excludes any involvement of excited HCl(v) side reaction. This is in accordance with rapid and complete relaxation of HCl(v) in our reaction system due to its relatively long reactor residence time: 0.26−1.22 s. The H atom concentration is too low to measure directly, but its change can be calculated from the flow balance eq 1 as shown in Figure 2. Its initial concentration $[H]_0$ be calculated from eq 2 as shown in Figure 3.

To obtain measurable signal intensities at $m/e = 1$, high H atom concentrations, the order of $10^{14}-10^{16}$ atoms/cm^3 would be needed,[14] which is outside the Knudsen flow limit of our system. Therefore, $[H]_0 \leq 7.24 \times 10^{11}$ atoms/cm^3—including the small background H atom concentration—was used.

The initial reactant concentration ratios $[Cl_2]_0/[H]_0$ were varied from 0.9 up to 26.7. In this wide range, the H atom consumption varies between 0.5×10^{11} and 5×10^{11} atoms/cm^3. These changes well describe the kinetics of reaction 1 according to eq 2a as displayed in Figure 4. All measured data points fit one line regardless of the exit orifice size. The measured rate constant k_1 is 10% lower than we had reported[1] earlier, where the H atom reactant was supplied by the background H atom concentration alone. That permitted us to make measurements only in narrow ranges of both the H atom and Cl_2 concentrations. The k_1 value represents a relatively slow rate for reaction 1. Combining it with our estimated[1] $A_1 = (1.6 \pm 0.6) \times 10^{-10}$ cm^3/(molecule-s), it gives 1.8 kcal/mol for the activation energy.

The microwave decomposition of HCl also has a prospective advantage for the kinetic investigation of radical cracking reactions. This method generates both H and Cl atoms. Substituting Cl_2 flow for C_2H_6, C_2H_5 radicals are formed in the reaction $Cl + C_2H_6 \rightarrow HCl + C_2H_5$ which then further react with H atoms establishing the $H + C_2H_5 \rightarrow 2CH_3$ cracking reaction. The $H + C_2H_6 \rightarrow H_2 + C_2H_5$ side reaction is insignificant at 298 K. Preliminary experimental results show significant CH_3 radical formation at $m/e = 15$. Introducing Cl_2 as a third component flow into the reactor, CH_3 radicals are partially converted into CH_3Cl recorded at $m/e = 50$ and 52 MS. Although the initial H and Cl concentrations cannot be varied independently, this is the only method known so far which permits the kinetic investigation of the ethyl radical cracking reaction at room temperature.

Earlier applications of HCl decomposition for H atom source have used ^{60}Co γ-radiolysis[15] of gaseous HCl and the photolysis of HCl using 184.9 nm wavelength of a low-pressure Hg lamp.[16] Both made measurements of k_1 relative to the $H + HCl \rightarrow H_2 + Cl$ reaction. The reported k_1/k_{-3} values are 115 and 93, respectively. Taking the value[9] of k_{-3} for the absolute rate calculation, $k_1 = 4.7 \times 10^{-12}$ and 3.8×10^{-12} cm^3/(molecule-s) are obtained. They are the lowest values reported for k_1.

The microwave decomposition of H_2 generates a complicated reaction system. In our case it involves reactions 1, 2, equilibrium 3, and the energy transfer reaction $H^*_2 + H$. In fast flow systems, where the contact time is around 2−15 ms, reaction

$$H + HCl(v) \xrightarrow{4} H_2 + Cl$$

has to be included. The number of rate constants involved, as well as unknown concentrations of H^*_2 and HCl(v) reactants create immense technical difficulties for a precise kinetic investigation.

In our experiments, the initial concentration ratios of reactants $[Cl_2]_0/[H]_0$, where $[H]_0 = 2([H_2]_I - [H_2]_0)k_{eH_2}/k_{eH} + [H]_b$, are varied from 0.74 up to 10.78. The kinetics cannot be described by eq 2 in that wide range of initial conditions as shown in Figure 7. However, the point-by-point differentiation of this curve reproduces the entire range of k_1 values reported from investigation employing the same H_2 decomposition technique (see Table 1 of ref 1).

Kinetic perturbation by side reactions has long been recognized and several attempts were made to find the exact stoichiometry of that complex mechanism. Mass balance equation $\Delta[H] + \Delta[H_2] = \Delta[Cl_2]$ found[3] can also be derived for our system in the form $\Delta[H]k_{eH} + \Delta[H_2]k_{eH_2} = \Delta[Cl_2]k_{eCl_2}$ by combining eqs 5 and 7 with the steady-state flow equation of H atoms. But it is actually equivalent to the overall flow balance presented in Figure 5. It is not an explicit indicator of the side reactions. Rather the difference between HCl and Cl product distributions shown in Figure 6 and its direct connection to H_2 consumption according to eq 10 are the direct consequences of an extended mechanism. The work of Ambidge et al.[17] takes into account the $H + HCl(v)$ side reaction only. Since the residence time of their system is short (<8 ms) and $[Cl_2]_0/[H]_0$ ratios are low, reaction 4 is probably the most significant side reaction. They report[17] $k_1 = (7.7 \pm 2.2) \times 10^{-12}$ cm^3/(molecule-s) at room temperature. Within this large scatter, it agrees with our present k_1 value.

No rate measurement for reaction 2 is reported in the literature. Our measured rate constant shows that this reaction is 1800 times faster than the thermal reaction 3. Also, our k_2 value is within the range of reported[9,10,18] A_3-factors range from 2.4×10^{-11} to 3.7×10^{-11} cm^3/(molecule-s). This indicates that the 12.6 kcal/mol (4400 cm^{-1}) excitation energy of $H_2(v = 1)$ provides the 4.4−4.6 kcal/mol activation energy of the thermal reaction 3.

The initial concentration of $H_2(v = 1)$ is small. It represents only 5% of $[H_2]_i$. This ratio is close to the ~4% value[10] estimated from the shift in the Lyman absorption bands of H_2. Reaction 2 is a considerable source of H atom recovery and of extra HCl product formation.

Rate constant derived for the $H + H_2(v = 1)$ energy transfer reaction is lower by 40% than that reported[13] in the literature. But our rate constant $k_{tr} = (2.95 \pm 0.17) \times 10^{-12}$ cm^3/(molecule-s) is derived independently from the thermal rate of the above H atom exchange reaction, while the earlier data[13] is bound to one of the reported[19] $k_H = 5.6 \times 10^{-10} \exp[(-8300 \pm 400)/RT]$ values for the $H + H_2$ thermal reaction. Despite numerous experimental and theoretical efforts, there is no consensus on the rate parameters of this thermal H atom exchange reaction. Theoretical calculation according to the variational transition theory combined with quantum dynamic coupling for accurate account for tunneling in the 200−300 K range[20] gives $k_H = (3.61 \pm 1.24) \times 10^{-12} \exp[(-4940 \pm 160)/RT]$ cm^3/(molecule-s). Comparison of our k_{tr} rate constant with that theoretical k_H value shows that the H exchange reaction is 3300 times faster with $H_2(v = 1)$ than with thermal H_2 at room temperature. The value of the A_H-factor is in good agreement with our k_{tr} which indicates that the $H_2(v = 1)$ excitation energy provides the entire activation energy requirement for the $H + H_2$ exchange process.

Both reaction 2 and the energy transfer process occur with the participation of the excited $H_2(v = 1)$. There are no other product formation channels, that is no branching that would be affected by the excitation. The rate constants are in good agreement with the A-factors of the corresponding thermal processes. It indicates that E_{vib} is effective in providing the activation energy, E_a, determined for the thermal reactions; $E_a - \alpha E_{vib} = 0$. With the reasonable assumption that $A_v = A$, the vibrational efficiency factor can be calculated[21] as $\alpha =$

$RT \ln(k_v/k)/E_{vib}$ which gives $\alpha_2 = 0.36$ and $\alpha_{tr} = 0.38$. Since $\alpha_2 \approx \alpha_{tr}$, it indicates that the energy transfer reaction occurs rather via H atom exchange than collisional deactivation.

Conclusions

Microwave decomposition of HCl is the most convenient method of H atom generation for the kinetic investigation of reaction 1 in the VLPR system. The relatively long residence time ensures the complete relaxation of excited HCl(v) product reducing thereby the reaction mechanism to the single-step thermal process of H + Cl_2. Wide range changes in reactant concentrations as well as residence time alterations provide an accurate rate constant measurement for $k_1 = (8.66 \pm 0.18) \times 10^{-12}$ cm^3/(molecule-s) at 298 K, in good agreement with total mass balance changes. Investigation performed under real second-order kinetics also permits the exact determination of the small background concentration of H atoms, $[H]_b = (7.2 \pm 0.2) \times 10^{10}$ atoms/cm^3, arising from the operation of the H_3PO_4 coated microwave discharge tube.

Due to the dual H and Cl atom generation, this method has a prospective kinetic application for the investigation of ethyl radical cracking by initiating both the Cl + $C_2H_6 \rightarrow$ HCl + C_2H_5 and H + $C_2H_5 \rightarrow 2CH_3$ reactions in our system.

H atom generation by the microwave decomposition of H_2 introduces a number of complexities. 5% of the initial H_2 concentration is converted into $H_2(v = 1)$ starting up therewith the reaction 2 in competition with the energy transfer quenching reaction H + $H_2(v = 1)$. Neglecting these side reactions, the kinetics of reaction 1 cannot be described by a single-step mechanism. But, as shown in Figure 7, such simplification reproduces the entire range of reported k_1 values derived from measurements with the use of the same H atom generation technique.

Using our present k_1 value, the kinetics for reactions of Cl and H atoms with excited $H_2(v = 1)$ reactant can be resolved. The derived rate constants are $k_2 = (2.88 \pm 0.13) \times 10^{-11}$ and $k_{tr} = (2.95 \pm 0.17) \times 10^{-12}$ cm^3/(molecule-s). Both rate constants agree well with corresponding *A*-factors reported for the thermal reactions.

Acknowledgment. Acknowledgment is made to the donors of the Petroleum Research Fund administered by the American Chemical Society, for the support of this research. We are also indebted to Professor Irving S. Reed of the Electrical Engineering Department at USC for a gift in support of the present work.

References and Notes

(1) Dobis, O.; Benson, S. W. *J. Phys. Chem.* A **2000**, *104*, 777.
(2) Kita, D.; Stedman, D. H. *J. Chem. Soc., Faraday Trans.* 2 **1982**, *78*, 1249.
(3) Stedman, D. H.; Steffenson, D.; Niki, H. *Chem. Phys. Lett.* **1970**, *7*, 173.
(4) Dobis, O.; Benson, S. W. *J. Phys. Chem.* **1995**, *99*, 4986.
(5) Dobis, O.; Benson, S. W. *Int. J. Chem. Kinet.* **1987**, *19*, 691.
(6) Dobis, O.; Benson, S. W. *J. Am. Chem. Soc.* **1991**, *113*, 6377.
(7) Albright, R. G.; Dodonov, A. F.; Lavrovskaya, G. K.; Morozov, I. I.; Tal'roze, V. L. *J. Chem. Phys.* **1969**, *50*, 3632.
(8) DeMore, W. B.; Sander, S. P.; Golden, D. M.; Hampson, R. F.; Kurylo, M. J.; Howard, C. J.; Ravishankara, A. R.; Colbe, C. E.; Molina, M. J. Chemical Kinetics and Photochemical Data for Use in Stratospheric Modeling. Evaluation Number 12. JPL Publication 97-4, 1977. Atkinson, R.; Baulch, D. L.; Cox, R. A.; Hampson, R. F.; Kerr, J. A.; Rossi, M. J.; Troe, J. *J. Phys. Chem. Ref. Data* **1997**, *26*, 521.
(9) Baulch, D. L.; Duxbury, J.; Grant, S. J.; Montague, D. C. *J. Phys. Chem. Ref. Data* **1981**, *10*, 1, Suppl. 1. Spencer, J. E.; Glass, G. P. *J. Phys. Chem.* **1975**, *79*, 2329.
(10) Heidner, R. F.; Kasper, J. V. V. *J. Chem. Phys.* **1969**, *51*, 4163. Polanyi, J. C.; Sadovski, C. M. *J. Chem. Phys.* **1962**, *36*, 2239.
(11) Leone, S. R. *J. Phys. Chem. Ref. Data* **1982**, *11*, 953.
(12) De Martini, F.; Ducuing, J. *J. Phys. Rev. Lett.* **1966**, *17*, 117.
(13) Gordon, E. B.; Ivanov, B. I.; Perminov, V. E.; Balalaev, V. E.; Ponomarev, A. N.; Filatov, V. V. *Chem. Phys. Lett.* **1978**, *58*, 425.
(14) Michael, J. V.; Niki, H. *J. Chem. Phys.* **1967**, *46*, 4969. Strumin, V. P.; Dodonov, A. F.; Lavrovskaya, G. K.; Tal'roze, V. L. *Kinet. Catal.* **1966**, *7*, 610. Tal'roze, V. L.; Strunin, V. P.; Dodonov, A. F.; Lavrovskaya, G. K. *Adv. Mass Spectrom.* **1965**, *3*, 993.
(15) Davidov, R. S.; Lee, R. A.; Armstrong, D. A. *J. Chem. Phys.* **1966**, *45*, 3364.
(16) Jardine, D. K.; Ballash, N. M.; Armstrong, D. A. *Can. J. Chem.* **1973**, *51*, 656.
(17) Ambidge, P. F.; Bradley, J. N.; Whytock, D. A. *J. Chem. Soc., Faraday Trans. 1* **1976**, *72*, 1157.
(18) Kumaran, S. S.; Lim, K. P.; Michael, J. V. *J. Chem. Phys.* **1994**, *101*, 9487.
(19) Gordon, E. B.; Ivanov, B. I.; Perminov, A. P.; Medvedev, E. S.; Ponomarev, A. N.; Tal'roze, V. L. *Chem. Phys.* **1975**, *8*, 147.
(20) Garrett, B. C.; Truhlar, D. G.; Schatz, G. C. *J. Am. Chem. Soc.* **1986**, *108*, 2876.
(21) Birely, J. H.; Lyman, J. L. *J. Photochem.* **1975**, *4*, 269.